

The Effects of Travel Speed of Tungsten Inert Gas Cladding of Tungsten Carbide and Nickel Composites on the Microstructure of Stainless Steel

Aws Ali Oleiwi^{1*}, Abdul Sameea Jasim Jilabi¹

¹ Faculty of Materials Engineering, University of Babylon, Hillah, Babil, Iraq

* Corresponding author's e-mail: aousali200@gmail.com

ABSTRACT

The scientific and industrial communities now consider surface modification of steel-based alloys to be essential. One effective method of altering these alloys' surfaces is tungsten inert gas (TIG) cladding. The purpose of this study is to investigate how the surface characteristics of austenitic stainless steel substrates are affected by TIG-deposited composite coatings made of tungsten carbide and nickel (WC-Ni). The study also intends to investigate the influence of the WC-Ni composite coatings' travel speed, and as a result, the heat input usually has significant effects on the microstructure. The coating layers were deposited at different travel speeds (67, 107, and 122 mm/min) using pre-placed composite pastes that were 1 mm thick and contained the same weight percentage of WC (65). The clad layers showed a variety of microstructures in optical and scanning electron microscopy, primarily nickel solid solution dendrites with WC particles scattered throughout the matrix. The dendrites at various locations across the clad layers were few or dense, finer or coarser, equiaxial or columnar, densely or less densely branched, depending on the cooling rates and the density of WC in the composite. Energy dispersive spectroscopy demonstrated that the Fe element that was transferred from the substrate material to the molten pool was primarily concentrated in the matrix, not the dendrites, while the dendrite locations and orientations were amply demonstrated by the distribution of the W element.

Keywords: surface modification, TIG cladding, Ni/WC composite coatings, travel speed.

INTRODUCTION

Stainless steels are important alloys owing to their distinctive and demanding characteristics. The variety of applications based on their use demonstrates their importance from simple ones, such as kitchenware and furniture, to extremely complex ones, like spacecraft and construction applications. Because of their durability and resistance to corrosion, thinner and more robust constructions are now conceivable. They are strong, hygienic, versatile, and recyclable while also offering a wide variety of shape, color, and form options [1, 2].

Three main types of microstructures exist in stainless steels, i.e., ferritic, austenitic, and martensitic. Out of these three main microstructures, stainless steels may be categorized into

several main classes. These are ferritic, austenitic, martensitic, duplex and precipitation hardening stainless steels [1]. Their physical, chemical, and mechanical properties vary depending on the chemical composition but each is characterized by the ability to form a self-healing protective oxide layer providing corrosion resistance, and a higher chromium content enhancing corrosion and oxidation resistance [3]. For instance, regarding these various properties, fully austenitic stainless steels are non-magnetic, but their martensitic and ferritic counterparts possess ferromagnetism [1]. The iron-based AISI 18-2Mn alloy, known as NITRONIC 32 (Nitrogen-strengthened austenitic stainless steel) contains primarily chromium and manganese. To attain particular qualities, varying amounts of nickel, molybdenum, niobium, vanadium, and/or silicon are also added. NITRONIC

32 offers about twice the yield strength of type 304, strong elevated-temperature strengths, low magnetic permeability, and excellent cryogenic properties [4]. Recently, surface modification has become necessary for the scientific community since the surface properties of new materials are usually inadequate in terms of wettability, adhesion, corrosion resistance, or even drag reduction. Moreover, for various reasons, it is difficult to find an alloy with a surface behavior different from that of the bulk. Surface modification has become an essential for more resistance to corrosion and wear, higher mechanical and fatigue resistance, better thermal (for low or high-temperature exposure), magnetic, electrical or specific optic or light exposure behavior. It is also vital for hydrophobicity, oleophobicity, or to create biocompatibility or (bio) fouling or even their combined effect. In order to achieve and improve these properties in metals and alloys, it is necessary to apply a surface modification strategy based on direct action on the metal, to build a coating provides these properties or to functionalize its surface for complex requirements [5].

Surface modification falls under two categories: physical and chemical. Physical modification results in a change in the topography or morphology of the surface with little or no change in the chemistry, such as etching, grit-blasting, and machining. Well-established chemical techniques include plasma and chemical vapor deposition, atomic layer deposition, and electro-chemical deposition. Chemical treatment can result in surface oxidizing/nitriding/carbiding, ion infusion, single layer coatings, or coatings comprising many layers of different compositions [6].

TUNGSTEN INERT GAS WELDING

In contrast to other arc welding techniques, gas tungsten arc welding (GTAW) – sometimes called as TIG-creates the arc using a non-consumable tungsten electrode. In GTAW, the weld puddle and heat input can be controlled considerably more precisely, because the arc and filler wire are independent of each other. In addition, there is less spatter with this technique, since the procedure does not require the molten filler metal to pass through the arc. It may produce better quality welds since it typically employs an inert gas for shielding. It can also give the option of welding without filler metal in specific circumstances [7].

This technique is a versatile and precise welding process that has found wide applications in various industries from aerospace to automotive. Its ability to weld thin and delicate materials with minimal distortion makes it a popular choice for demanding welding applications [8]. Because it can be used at very low current and without the addition of a filler metal, it is often used for small components where heat generation is a problem. The medical devices and electronic industries use GTAW extensively for final closure welds on sensitive products such as pacemakers and batteries. It can also be used to make pipes, and commonly used in the manufacture of heat exchangers. GTAW is a popular process for a variety of repair welds because the heat input can be precisely controlled and directed, such as in the gas turbine engine industry. In general, GTAW is often the process of choice when high quality welds and precise heat control are required [7].

TUNGSTEN INERT GAS CLADDING

The TIG coating process (Figure 1) is typically used to increase hardness, wear resistance and enhance the surface properties of a substrate by accumulating or adding a new layer on the substrate surface. There are some other common coating processes such as electron beam coating and laser coating, which modify the surface properties by melting the substrate layer and powder coating layer at the same time. However, the variable absorption rate of laser beam in different coating powders limits the use of laser cladding, and complex components made by laser cladding are expensive and require advanced equipment. Fortunately, TIG cladding offers a higher deposition rate, ease of operation and lower equipment and maintenance costs than other cladding techniques [9].

Advantages and limitations of the TIG cladding

The TIG cladding technique features high-level precision control, low health risks and less spattering. It also produces good bead appearance, has great flexibility of application and is relatively low cost. Compared with carburizing and nitriding, the TIG arcing technique has the ability to alter the surface to a higher depth (mm range) [11]. It however has a low travel speed compared to other techniques such as laser coating [11, 12].

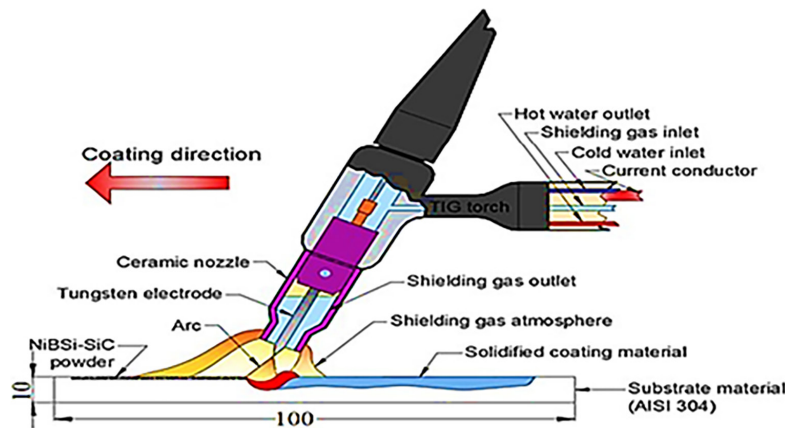


Figure 1. Schematic representation of the principle work of the TIG cladding [10]

METAL MATRIX COMPOSITE COATING

In any engineering component, surfaces are first exposed to friction, thermal, mechanical, chemical and/or electrochemical effects, leading to damage the components in industry. This damage cannot be repaired if the tribological and corrosion phenomena are not adequately controlled using the right surface technique; the damage can be avoided or at least delayed. Therefore, surface coating technique is more effectively used to increase hardness, wear resistance, corrosion resistance and high temperature resistance without changing the properties of the substrate. Nowadays, coatings that exploit the high hardness and strength of the ceramic phase, and sound toughness of the matrix to produce a metal matrix composite (MMC) layer are widely used for repairing of surface and strengthening of engineering metal components. The MMC coating technique of adding reinforcing particles can be easily achieved using the TIG cladding [13]. The reinforcement phases within the matrix phase might resemble fibers, whiskers, sheets or particles. Ceramic carbides, nitrides, borides and oxides are examples of reinforcing materials. MMCs are often fabricated from lightweight, low-density metals such as Al, Mg, Cu, Ni, or Ti, which are superior to unreinforced metals in terms of specific stiffness and strength-to-weight ratio, service temperature, wear and corrosion resistance [14].

TUNGSTEN CARBIDE REINFORCED METAL MATRIX COMPOSITES

In general, compared to unreinforced metals, MMCs reinforced with particles or fibers of a

ceramic material such as silicon carbide or graphite offer higher specific strength and hardness, higher service temperature, and greater wear resistance, in addition to the ability to tailor these properties to a specific application [15]. However, fabrication of entire MMCs is considered wasteful and uneconomical due to the complexity of manufacturing in addition to the high cost of the reinforcement ceramic particles [16]. Surfaces can be coated with non-metallic or metallic compounds to improve adhesion (wettability) and mechanical properties. Adding the optimal quantity of hybrid reinforcements increases hardness and tensile strength by up to 30% and 40% respectively, when compared to a composite with the same quantity of single reinforcement [17].

Despite the fact that various hard ceramics have been successfully used as particle reinforcement in MMCs, tungsten carbide (WC) has been shown to be a promising choice as a coating in various structural components. This is due to its interesting physical and mechanical properties such as high melting point, exceptional hardness, low coefficient of friction, chemical inertness and resistance to oxidation [18]. WC occupies a leading position in industrial applications as it is one of the most suitable reinforcements for iron matrices because of its availability, high hardness (HV0.1~2280) and good thermodynamic stability [19].

Recently, laser cladding has been used to produce wear-resistant layers based on metallic and composite materials such as MMCs based on nickel matrix reinforced by WCs [20]. The higher scan speed of the laser cladding means that less metal powder is injected into the weld pool, so the cladded track is thinner with reduced HAZ depth, but the clad micro-hardness increases [21].

Although these particular advantages, applying laser surface modification is improper in industries due to the complexity of the technique, high initial capital expenditure, demand for skilled operators and necessity for surface preparations in challenging terrain [22]. Alternatively, TIG cladding is a low cost technique for depositing thick coating layers, due to its ease of use and low setup cost [23, 24]. It is evident that in addition to laser cladding technique, TIG cladding has received popularity to produce a hard clad layer on different graded substrate materials [25]. However, the layer deposited by the TIG cladding has a thickness of almost twice that deposited by laser [26, 27].

The main problem with laser deposition is the formation of defects such as cracks, spalling, holes, porosity and thin interface. This can be reduced by using the TIG technique. Preheating the base substrate is generally used to reduce the risk of cracking [28, 29]. Abrasive wear is a common problem in industrial components, reducing the life and performance of equipment and machinery. Therefore, WC-based cermet coatings have been used in critical applications to overcome this problem [30].

TIG cladding was used to deposit the WC coating on AISI 4340 steel and for the Ni-WC powder coating on AISI 1010 steel [31, 32]. To improve the hardness and wear resistance of AISI 1050 steel, TIG cladding was used to deposit the multi-pass coating of WC on the substrate. The results revealed that the hardness was improved, whereas the wear performance was reduced due to the transfer of the metastable phase to a stable phase under specific sliding conditions [33]. Ni was usually added to WC coating to improve crack resistance [34], as Ni and Fe have excellent compatibility [35]. Due to the poor electrical conductivity of carbides, a pre-applied coating layer of pure carbide ceramic particles such as (WC, TiC, SiC, etc.) may induce arc interruption during the TIG coating process, decreasing the process efficiency [36]. The adding the right bonding metal to the carbide particles, the overall amount of heat input to the substrate is reduced, potentially minimizing the heat affected zone (HAZ) width and thermal stress induction in the substrate [37]. The increased

solubility of carbides in the nickel matrix at higher temperatures (in the molten state) improves the bond strength between the carbide particles of the coating and the substrate, further increasing wear resistance [38]. Several studies have been carried out to improve the strength of the WC reinforced MMC coating by Ni or Ni-based matrix as a binding material for various high energy density techniques [39, 40]. The combination of Ni with the hard carbide particles improves the surface characteristics of the generated components, because of the Ni greater wettability [41]. The microstructure and mechanical behavior are significantly impacted by the current and scan speed of the arc when using TIG cladding technique in Carbide-Ni composite coatings produced [42].

MATERIALS AND THEIR SPECIFICATIONS

In this experiment, an austenitic stainless steel AISI 18-2Mn plates with the dimension of (10×70) mm. The chemical composition of the austenitic stainless steel plates used in this study as substrates according to the American Iron and Steel Institute (AISI) [4] is shown in Table 1. The pieces (substrates) to be coated were prepared from the raw material with a length of (100 mm) for each piece. The chemical composition analysis for the raw material was carried out using OXFORD instrument at Al-Razi Metallurgical Research Center-Tehran/Iran based on RMRC-WI-560-112-04. Table 1 shows the chemical composition (with an average of three readings) of the raw material used as a substrate. This composition conforms to AISI 18-2Mn Nitronic 32 (nominal).

CLADDING MATERIALS

Pure nickel powder

Table 2 showing the chemical composition analysis performed using XRF at Al-Razi Metallurgical Research Center-Tehran/Iran based on ASTM E 1621-21 revealed that the purity of Ni powder

Table 1. Nominal and actual chemical composition of the substrate material

Alloy		Chemical composition (wt.%)								Spec. symbol (AISI)
		C	Mn	Si	Cr	Ni	N	P	S	
A.S.S.	Nominal	0.15 max.	11.0-14.0	1.0 max.	16.5-19.0	0.5-2.5	0.2-0.45	0.045 max.	0.03 max.	18-2Mn (Nitronic 32)
	Actual	0.065	10.45	0.43	13.5	1.2	0.18	0.044	0.005	

Table 2. Chemical analysis of nickel powder

Element	Ni	Mg	Si
wt. %	99.64	0.2	0.16

was 99.64 wt.%. The particle size of Ni powder was analyzed using a Bettersize 2000 laser particle size analyzer located in the laboratories of Ceramic Engineering and Building Materials Department/Faculty of Materials Engineering/University of Babylon. The particle size was 3.7–63.4 μm.

Tungsten carbide powder

The particle size of WC powder analyzed using the Bettersize 2000 laser particle size analyzer was 3–6 μm. Table 3 shows the chemical composition analysis of WC powder conducted using XRF at Al-Razi Metallurgical Research Center based on ASTM E 1621-21. The weight percent of C element in XRF analysis has been calculated by stoichiometry according to the XRD result.

Binding material

Polyvinyl alcohol (PVA) was used as a binder material to make a pre-placed WC-Ni composite paste. Table 4 shows the specifications of PVA, according to ME Scientific Engineering Ltd. product of Germany, packed in the UK.

PROCEDURES BEFORE THE CLADDING PROCESS

The following procedures have been carefully carried out before the start of the cladding process:

1. Cleaning the substrate surfaces from oils, grease and other impurities.
2. Eight slots with dimensions of (1×6×30 mm) were made in the substrates (Figure 2a) using a universal milling machine, inside which the pre-placed

Table 3. Chemical analysis of tungsten carbide powder

Element	W	C
wt. %	93.87	6.13

Table 4. Polyvinyl alcohol specifications

Product	PVA code	Molecular formula	Viscosity
MESE	8–88	(C ₄ H ₆ O ₂ .C ₂ H ₄ O) _x	8 mPa.s (in 4% aqu. Solution)

WC-Ni composite coatings were deposited.

3. To prepare the binder, 4.0% of PVA was dissolved in 96% of hot distilled water (50 °C) for 15 min. using a magnetic stirrer located in the laboratories of the Metallurgical Engineering Department/Faculty of Materials Engineering/University of Babylon.
4. Different wt.% of WC powder (35, 50, 65, 80 and 95) and Ni powder were weighed using a sensitive balance in the laboratories of the Metallurgical Engineering Department to be then mixed as WC-Ni mixtures.
5. To keep the powder mixtures under the flow of Ar gas during TIG cladding, these mixtures were blended with a 4.0% PVA solution binder to form a pre-placed WC-Ni composite paste to be subsequently deposited in the slots (Figure 2b).

TUNGSTEN INERT GAS CLADDING OF TUNGSTEN CARBIDE-NICKEL COMPOSITE COATING ON AUSTENITIC STAINLESS STEEL SUBSTRATE

The cladding process was carried out using a TIG welding machine combined with a lathe machine to make the tungsten arc travels along the composite layers at automatic and constant speeds. The arc ignition and extinguishing were on the substrate for each coating layer (Figure 3). Table 5 shows the TIG cladding parameters based on the trial and error method and previous literature.

RESULTS AND DISCUSSION

The results of the experimental work were presented and discussed. Microanalysis of MMC coatings deposited on austenitic stainless steel substrates have been evaluated by the OM, SEM with the assistance of the EDS.

Macroscopic metallography

Before discussing the microstructural variations across the coated samples, it is necessary to get acquainted with the microstructure of the

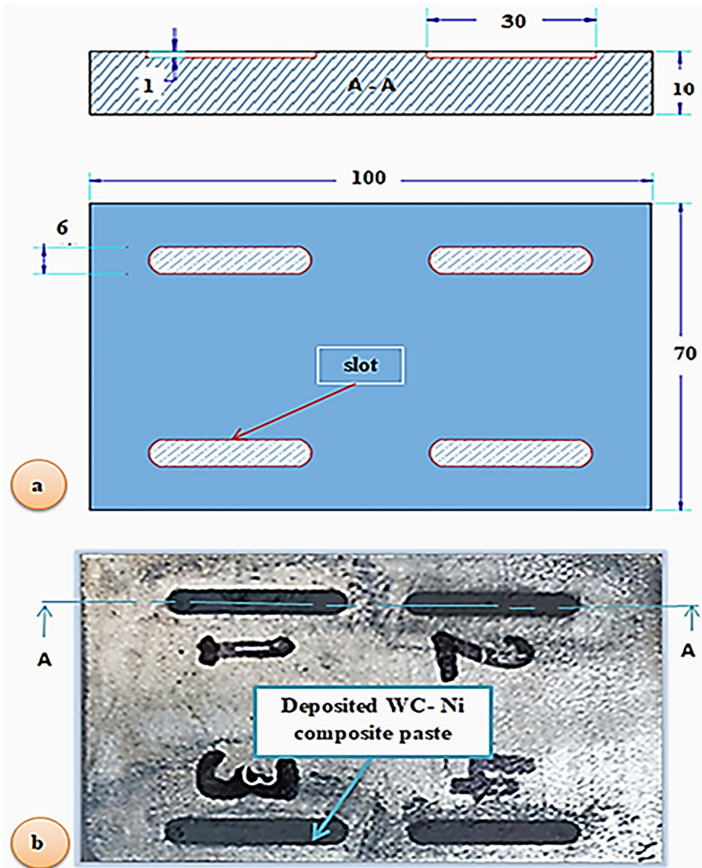


Figure 2. (a) Dimensions of slots machined in the substrates in mm
(b) WC-Ni composite paste deposited in the slots

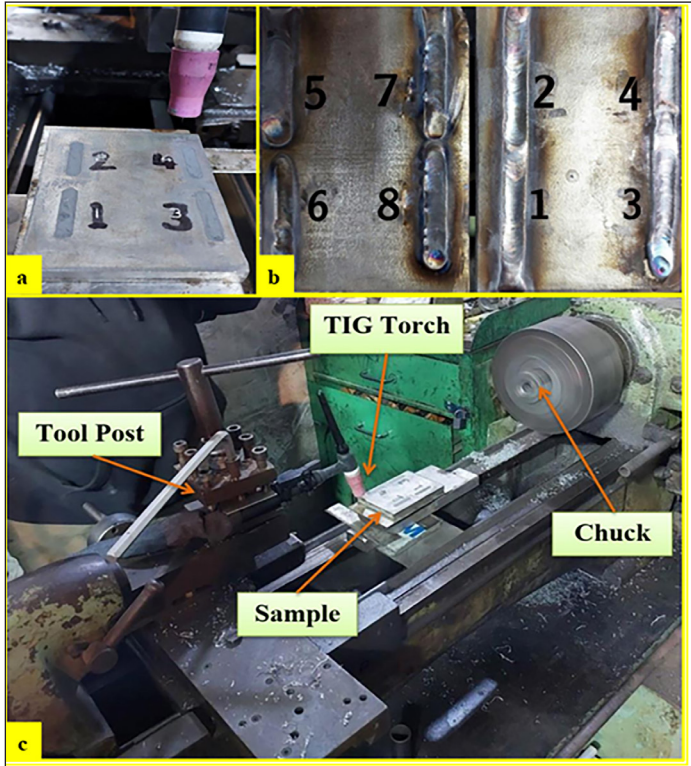


Figure 3. (a) Samples under cladding (b) samples before preparing test specimens (c) the TIG torch combined with a lathe machine

Table 5. TIG cladding parameters of austenitic stainless steel substrates

Cladding by the use of	Pure WC powder of (wt.%)		
	65		
Clad symbol	C1	C2	C3
Travel speed (mm/min.)	67	107	122
Current value (A)	130		
Arc voltage value (V)	15		
Position	Flat		
Polarity	DCEN		
Thickness of layer (mm)	1		
Ar gas flow rate (l/min)	10		
Ar gas purity (%)	99.999		
Arc length (mm)	3		
Tungsten electrode diameter (mm)	2.4		
Tungsten electrode type	Thoriated tungsten ESAB-WT20		

substrate material prepared from AISI 18-2Mn austenitic stainless steel. OM and SEM show in Figure 4 that the microstructure of the substrate alloy was austenite grains noting the appearance of twinning. Table 1 shows the chemical composition of this steel possessing high contents of Mn (up to 10.45 weight percent) and N (up to 0.18 weight percent), which partly replace Ni as austenite stabilizers. This is the reason why austenite grains appear on microscopic examination [43]. Since N has more solubility than carbon in austenitic iron and is a stronger austenite stabilizer and solid solution strengthener without significantly reducing fracture toughness, it has advantageous properties [44].

According to studies [45, 46, 47], as the concentration of N increases, single and polycrystalline austenitic stainless steels exhibit a greater propensity to form planar dislocation structures. These structures lead to enhanced strain hardening through slip band formation and, in some

cases, deformation twinning by reducing the material’s ability to cross-slip [48]. So twinning can be clearly shown in the Figure 4.

Microscopy of each sample showed variations in microstructures of the clad layer and adjacent regions of the substrate. These variations are attributed to the differences in chemical compositions of the coating layers and the large thermal gradients to which the sample is exposed from the melting temperature to that of the substrate unaffected by heat. This is typically followed by a rapid cooling rate caused mainly by the relatively cold substrate and the atmosphere.

The effect of cladding travel speed

With the carbide-nickel composite coatings produced by the TIG cladding technique, the travel speed and as a result the heat input have typically significant effects on the microstructure [49]. Macroscopic examination was carried out

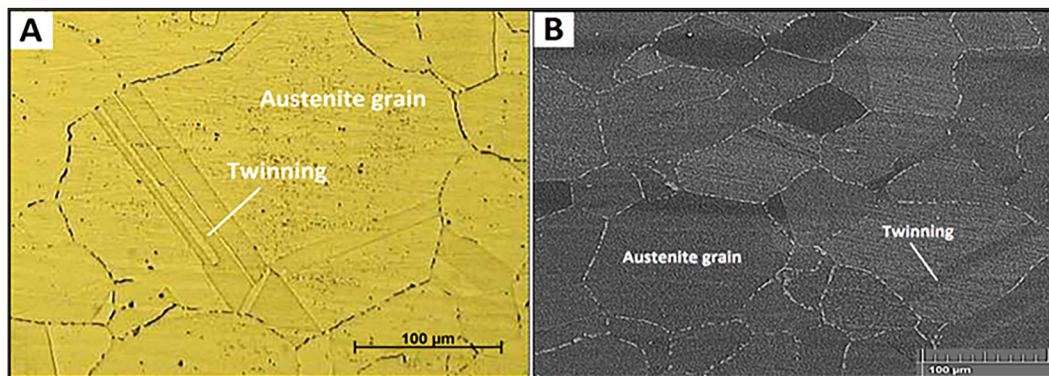


Figure 4. Microstructure of the substrate material using an (a) OM and (b) SEM

on three specimens of austenitic stainless steel substrates coated with WC-Ni composite by the TIG cladding technique using the same wt.% of WC (65%) and various travel speed values (67, 107 and 122 mm/min.).

Microscopy revealed in Figure 5 that dendrites are present at the different zones along the cross section of the C1 clad layer. This could be due to the wt.% of WC in the composite to 65%, which in turn presents the dendrite nuclei. The SEM also revealed equiaxed grains in Zone 1, and a mixture of equiaxed and columnar grains in Zone 2, while the columnar grains were predominant in Zone 3. The proportion of columnar grains increases while approaching the cooling surface of the clad-substrate interface. Figure 6 shows microstructures of the different zones at

higher magnifications. Table 6 exhibits that the EDS elemental composition analysis along the centerline of the cross section of the C1 clad layer was (53.9% Fe, 8.2% Ni, 20.0% W, 7.4% Mn and 10.5% Cr on average). It is noted that the average W content in this clad layer significantly increased. This is the reason behind the proportion of dendrites in this sample. However, the average contents of Fe, Mn and Cr in the clad layer were less. This confirms that the dilution with the substrate material in this sample was lower.

Figure 7 shows the EDS chemical composition analyzes of A and B regions indicated in the scanning electron microstructure of the Zone 1 of the C1 sample. It is clearly observed from the figure that there is a large discrepancy in the chemical composition analyzes of A and B regions due to

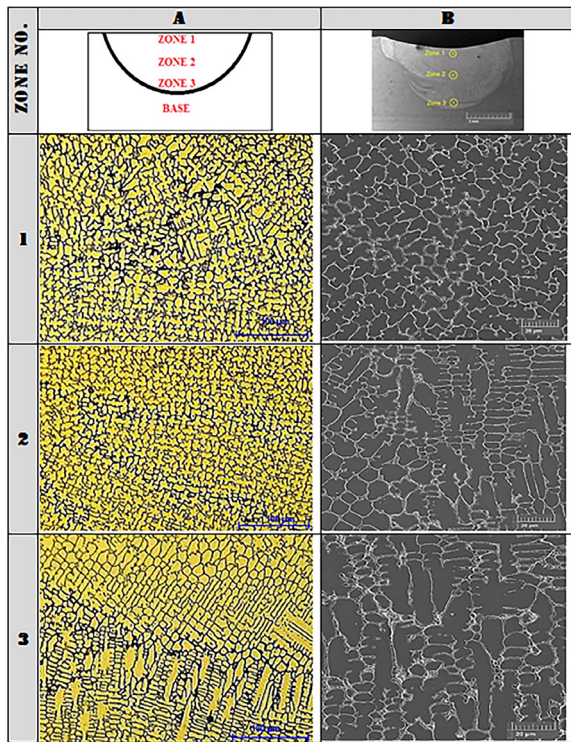


Figure 5. Microstructural map of the C1 sample at different depths along the centerline of the cross section of the clad layer using an (a) OM and (b) SEM

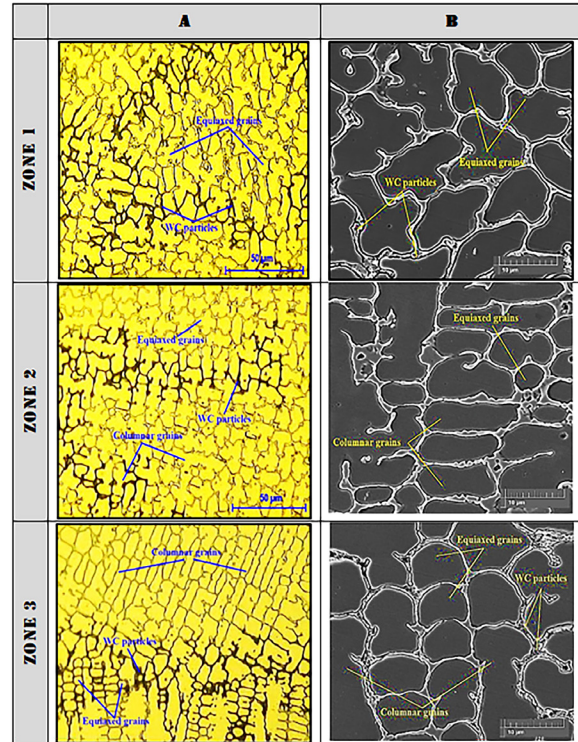


Figure 6. Microstructural map of the C1 sample at higher magnifications using an (a) OM and (b) SEM

Table 6. The EDS elemental composition analysis of the C1 sample at different depths along the centerline of the cross section of the clad layer

Element	Zone 1 [wt.%]	Zone 2 [wt.%]	Zone 3 [wt.%]
Tungsten	19.93	21.69	18.30
Nickel	8.55	8.38	7.62
Iron	54.01	52.47	55.36
Manganese	7.06	7.17	7.89
Chromium	10.45	10.30	10.83

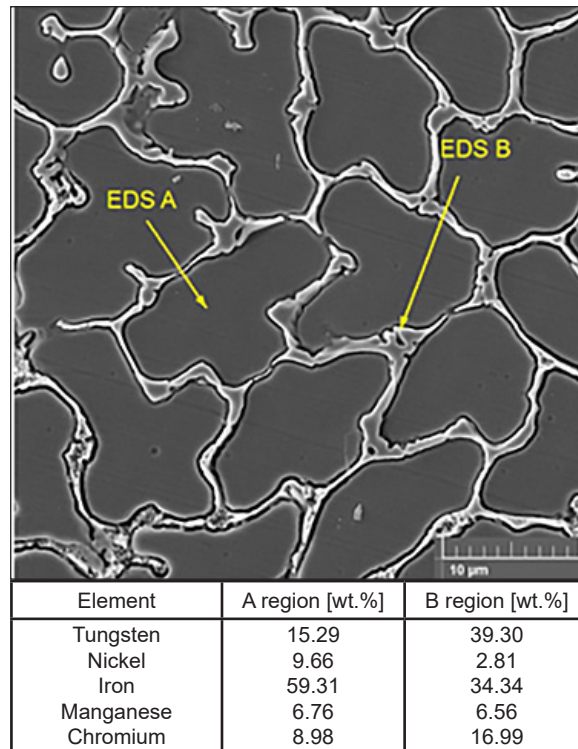


Figure 7. EDS elemental composition analysis of A and B regions indicated in the scanning electron microstructure of the Zone 1 of the C1 sample

the apparent heterogeneity in the microstructures of these different regions. The higher W element content at B region (dendrites) is due to the fact that the WC particles serve as nuclei for the dendrites, as mentioned earlier. On the contrary, the contents of Fe and Ni elements are greatly higher at A region (Ni-based matrix) indicating that the iron element is mainly concentrated in the matrix rather than the dendrites. However, the Cr wt.% in the dendrites region was much higher than in the matrix, while the Mn wt.% was similar.

The effect of increasing the cladding speed value to 107 mm/min on the microstructures of the clad layer (C2) at all three zones is shown in Figures 8 and 9 using OM and SEM. There was a marked increase in dendrites. The figures also show that the dendrites were mostly columnar in all three zones. The reason behind these

observations could be the higher cooling rates due to the lower heat input resulting from the higher travel speed used with this sample. It is clearly observed from the figures that the structure in Zone 2 is slightly finer than that in Zone 1, and that the columnar structure significantly increases while advancing towards the bottom of the clad layer. This might be due to the proximity of the cooling surface (clad-substrate interface). The EDS elemental composition analysis along the centerline of the C2 cross section shows in Table 7 that the content of each element has noticeably varied at the three test points with averages of 51.5% Fe, 9.2% Ni, 21.6% W, 7.3% Mn and 10.4% Cr. Obviously, the average iron content is still more than half of the total constituents of the clad layer due to the effect of dilution with the substrate material. However, compared

Table 7. The EDS chemical composition analysis of the C2 sample at different depths along the centerline of the cross section of the clad layer

Element	Zone 1 [wt.%]	Zone 2 [wt.%]	Zone 3 [wt.%]
Tungsten	24.16	23.34	17.39
Nickel	9.50	9.30	8.69
Iron	48.98	50.15	55.54
Manganese	7.07	7.07	7.60
Chromium	10.29	10.14	10.77

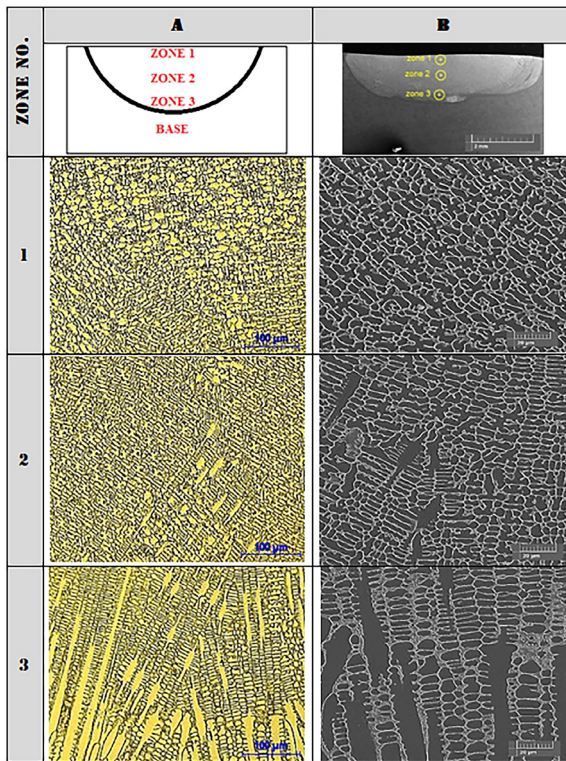


Figure 8. Microstructural map of the C2 sample at different depths along the centerline of the cross section of the clad layer using an (a) OM and (b) SEM

with C1 which has the same preplaced composite paste (65% WC-Ni), but with a travel speed of 67 mm/min, the dilution ratio in C2 sample is lower. This is due to the fact that increasing travel speed leads to a decrease in heat input [50]. Therefore, the dilution ratio of the substrate material elements (iron, chromium and manganese) decreases with increasing those of the coating (tungsten and nickel). It can also be noted from Table 7 that the substrate material elements in Zone 3 are clearly higher than those in Zones 1 and 2 at the expense of the coating elements. This is due to the dilution effect with the substrate material due to the proximity of this zone to the substrate.

With the increased TIG cladding travel speed value to 122 mm/min, the microstructure at each of the three zones along the cross section of the C3 sample is affected, where Figures 10 and 11 show the optical and scanning electron microstructures of this sample. It is clearly observed that the dendritic structure increased significantly at the expense of the matrix, and the columnar dendrites were generally more than those that appeared in the C2 clad layer. The reason for this might be that increasing the cladding

speed value definitely reduces the amount of heat introduced into this sample, which leads to increased cooling rates.

The figures also exhibit a distinct heterogeneity in the microstructures of the three zones. The microscopy generally showed densely branched dendrites of nickel solid solution with tungsten carbides segregated at the dendrite boundaries due to the growth of the dendrite branches, which all are distributed through the matrix. In Zone 3, the density of dendrite branches was higher, and the columnar dendritic structure was more. This is due to the effect of increased cooling rates to which this zone is exposed by the adjacent colder substrate material. Microstructural examination also showed in Zone 3 that the matrix noticeably increased at the expense of dendrites. The reason for this is that the dilution effect is greater in this zone due to its proximity to the substrate material.

Figure 10 and Table 8 show the EDS map and chemical composition analysis at different depths along the centerline of the C3 cross section. It is clearly observed from the table that the content of each element has also varied noticeably at the three test points with averages of 38.5% Fe, 16.6% Ni, 34.6% W, 5.2% Mn and 5.1% Cr.

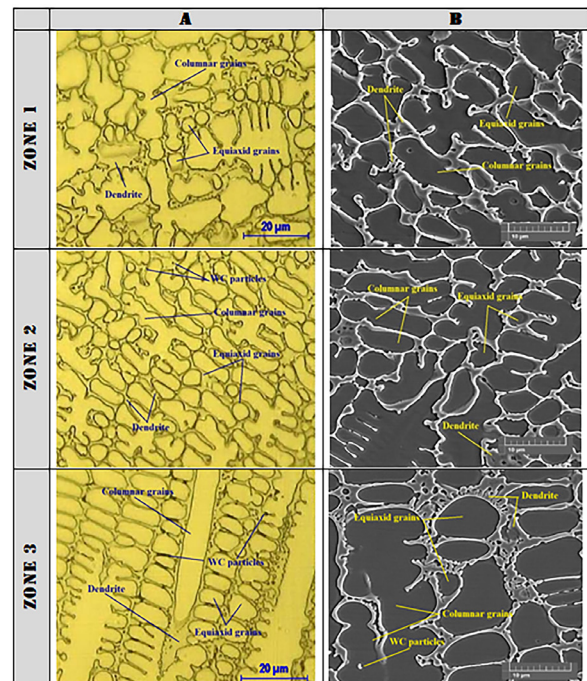


Figure 9. Microstructures of the C2 sample in the different zones at higher magnifications using an (a) OM and (b) SEM

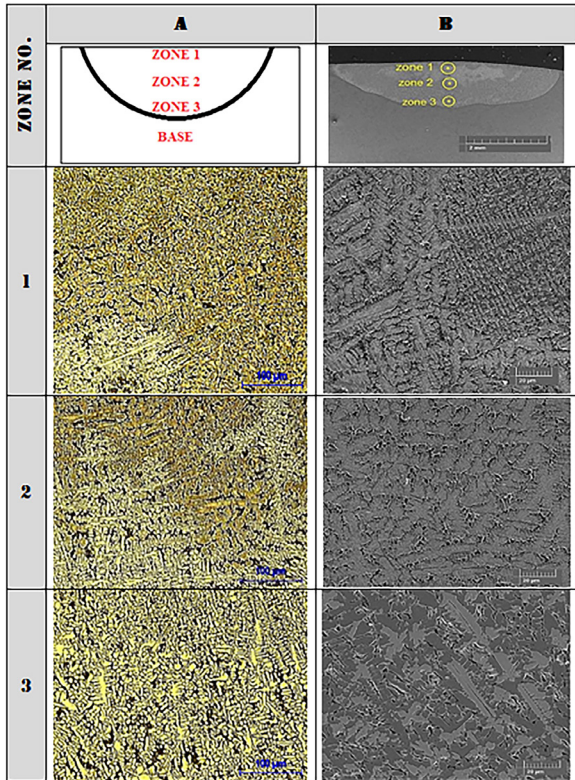


Figure 10. Microstructural map of the C3 sample at different depths along the centerline of the cross section of the clad layer using an (a) OM and (b) SEM

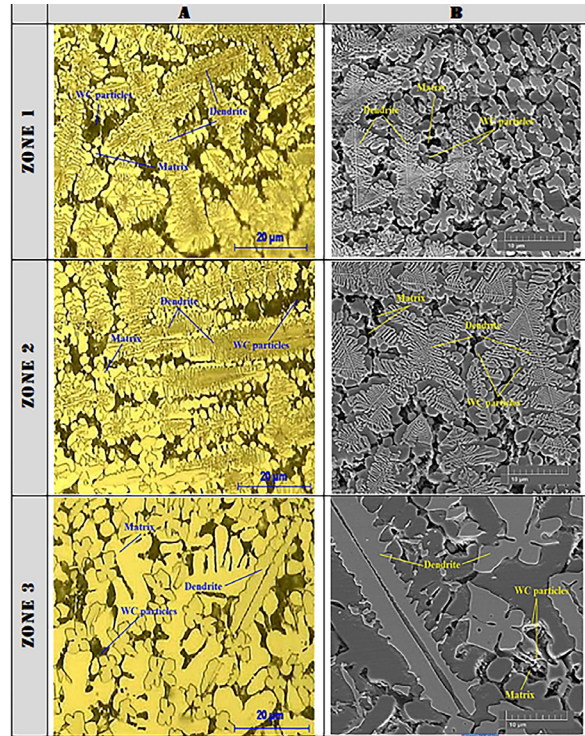


Figure 11. Microstructures of the C3 sample in the different zones at higher magnifications using an (a) OM and (b) SEM

This variation is accompanied by the heterogeneity in the microstructures of the different zones shown in Figures 10 and 11. The distribution of the W element at the three test points (Figure 12) clearly indicates the shapes, sizes and locations of the dendrites shown by SEM in Figure 11. While moving from Zone 1 towards Zone 3, the decrease in W content was associated with an increase in Fe content. This was accompanied by a noticeable increase in the matrix at the expense of the dendrites shown in the microstructural examination as a result of the increased dilution effect in this zone due to its proximity to the substrate material.

The distribution of the Ni, Fe and Mn elements clearly indicates (especially in Zone 3) the Ni-based matrix shown by SEM in Figure 11. The average iron content for the three test points is approximately 38.5% of the total constituents of the clad layer, proving that the dilution that occurred with the substrate material for this sample was lower than that occurred with the other samples discussed before. This is due to reduced fusion as a result of the increased TIG cladding travel speed used with this sample.

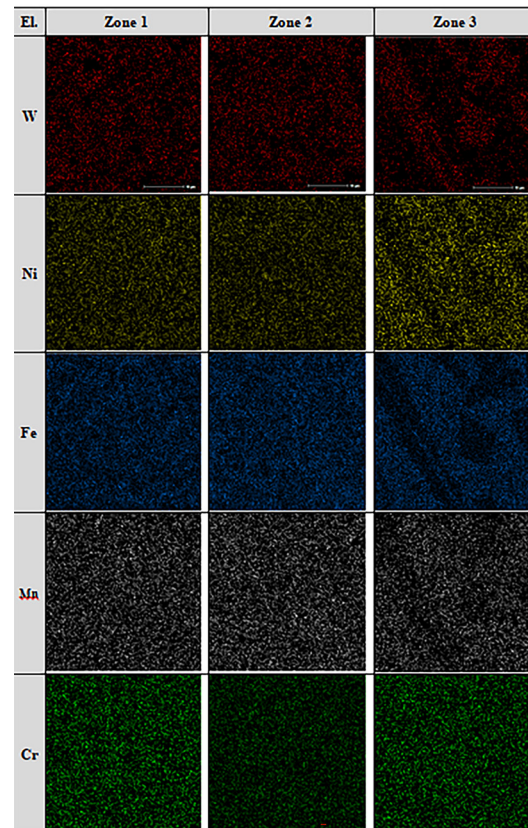


Figure 12. The EDS map of the C3 sample at different depths along the cross section of the clad layer

Table 8. The EDS chemical composition analysis of the C3 sample at different depths along the centerline of the cross section of the clad layer

Element	Zone 1 [wt.%]	Zone 2 [wt.%]	Zone 3 [wt.%]
Tungsten	37.94	34.89	30.95
Nickel	17.99	15.14	16.66
Iron	34.75	39.13	41.59
Manganese	4.66	5.28	5.63
Chromium	4.67	5.56	5.16

CONCLUSIONS

This study explored the effect of using wt.% of WC (65) and various travel Speeds (87, 107, and 122A) on WC-Ni composite coatings deposited on austenitic stainless steel substrates using TIG cladding technique. The most important results of this study can be concluded as follows:

- as a result of the travel speed that the TIG cladding technique produces, the heat input usually has a big impact on the microstructure;
- the microstructures of the C1 sample clad layer (65% WC-Ni and 87 A) were mainly composed of Ni solid solution grains with WC particles distributed through the matrix. There is a notable increase in the proportion of the Ni solid solution dendrites, which became somewhat mostly columnar while moving towards the bottom of the coating layer;
- increasing the travel Speeds to 107A. led to the formation of finer and mostly columnar dendrites across C2 clad layer;
- with C3 sample (122A. of travel Speed), the proportion of dendrites and carbides clearly increased at the expense of the matrix. The dendrites were also more densely branched.

Lessons learned from this study can be taken into consideration in studies on cladding, and some fields covered in this study could be further improved. The following is a summary of recommendations for further work.

1. A corrosion test can be carried out for the coating layers.
2. Laser cladding technique can be used.
3. More wt.% of WC might be in pre-placed composite pastes.
4. Studying the effect of the mass fraction of WC in WC-Ni composite coatings and welding current on the microstructure and properties of the clad layers.
5. Investigating the influence of particle size of pre-placed composite powders on the characteristics of the clad layers.

6. Cladding other substrate materials such as low alloy steel.

Acknowledgment

Author's thanks Dr. Abdul Sameea Jasim Jilab and Mr. Murtadha Mohsen Mottar Ali Al-Masoudy for their help and advice to complete this work.

REFERENCES

1. Lo K.H., Shek C.H., Lai J.K. Recent developments in stainless steels. *Materials Science and Engineering: R: Reports*. 2009, 65(4–6): 39–104.
2. Baddoo N.R. Stainless steel in construction: A review of research, applications, challenges and opportunities. *Journal of constructional steel research*. 2008, 64(11): 1199–206.
3. Rossi B. Discussion on the use of stainless steel in constructions in view of sustainability. *Thin-Walled Structures*. 2014, 83: 182–9.
4. Davis J.R. editor. *Stainless steels*. ASM international; 1994.
5. Rius-Ayra O., Llorca-Isern N. Surface modification of metals and alloys. *Coatings*. 2021, 11(2): 260.
6. Bose S., Robertson S.F., Bandyopadhyay A. Surface modification of biomaterials and biomedical devices using additive manufacturing. *Acta biomaterialia*. 2018, 66: 6–22.
7. Khan A. *Tungsten Inert Gas Welding (TIG) Principles, 6 Parts, Applications, Pros, Cons*. Dizz. 2018.
8. Kaulgud O.M., Chavan S.T. Process Parameter Optimization of TIG Welding by Taguchi Method and Its Effect on Performance Parameter of Stainless Steel Grade 302HQ. *International Transaction Journal of Engineering, Management, & Applied Sciences & Technologies*. 2022, 13(7).
9. Singh J., Thakur L., Angra S. Effect of argon flow rate and standoff distance on the microstructure and wear behaviour of WC-CoCr TIG cladding. In *Journal of Physics: Conference Series*. 2019, 1240(1): 012162. IOP Publishing.
10. Kilic M., Imak A., Kirik I. Surface modification of

- AISI 304 stainless steel with NiBSi-SiC composite by TIG method. *Journal of Materials Engineering and Performance*. 2021, 30(2): 1411–9.
11. Kumar S., Ghosh P.K. Thermal behaviour of TIG arc surfacing affecting mechanical properties of AISI 4340 steel substrate under static and dynamic loading. *Materials Science and Engineering: A*. 2020, 773: 138734.
 12. Davis J.R., editor. *Surface hardening of steels: understanding the basics*. ASM international; 2002.
 13. Karmakar R., Maji P., Ghosh S.K. A review on the nickel based metal matrix composite coating. *Metals and Materials International*. 2021, 27: 2134–45.
 14. Ashebir D.A., Mengesha G.A., Sinha D.K. An insight into mechanical and metallurgical behavior of hybrid reinforced aluminum metal matrix composite. *Advances in Materials Science and Engineering*. 2022.
 15. Chawla, K.K., Chawla, K.K. *Metal matrix composites*. Springer New York; 1998, 164–211.
 16. Yan H., Zhang P., Yu Z., Lu Q., Yang S., Li C. Microstructure and tribological properties of laser-clad Ni–Cr/TiB₂ composite coatings on copper with the addition of CaF₂. *Surface and Coatings Technology*. 2012, 206(19–20): 4046–53.
 17. Karthik B.M., Gowrishankar M.C., Sharma S.S., Hiremath P., Shettar M., Shetty N. Coated and uncoated reinforcements metal matrix composites characteristics and applications—A critical review. *Cogent Engineering*. 2020, 7(1): 1856758.
 18. Liu K., editor. *Tungsten carbide: processing and applications*. BoD—Books on Demand; 2012 Dec 19.
 19. Grairia A., Beliardouh N.E., Zahzouh M., Nouveau C., Besnard A. Dry sliding wear investigation on tungsten carbide particles reinforced iron matrix composites. *Materials Research Express*. 2018, 5(11): 116528.
 20. Lisiecki A., Ślizak D. Hybrid laser deposition of composite WC-Ni layers with forced local cryogenic cooling. *Materials*. 2021, 14(15): 4312.
 21. Farahmand P., Kovacevic R. Parametric study and multi-criteria optimization in laser cladding by a high power direct diode laser. *Lasers in Manufacturing and Materials Processing*. 2014, 1: 1–20.
 22. Jeyaprakash N., Yang C.H., Kumar D.R. Laser surface modification of materials. *Practical Applications of Laser Ablation*. 2020, 61–81.
 23. Hong C., Gu D., Dai D., Cao S., Alkhayat M., Jia Q., Gasser A., Weisheit A., Kelbassa I., Zhong M., Poprawe R. High-temperature oxidation performance and its mechanism of TiC/Inconel 625 composites prepared by laser metal deposition additive manufacturing. *Journal of laser applications*. 2015, 27(1).
 24. Kumar V., Lucas B., Howse D., Melton G., Raghunathan S., Vilarinho L. Investigation of the A-TIG Mechanism and the Productivity Benefits in TIG Welding. In 15th International Conference on the Joining of Materials (JOM 15) and 6th International Conference on Education in Welding (ICEW 6) Helsingor, Denmark 2009, 3–6.
 25. Prasad R., Waghmare D.T., Kumar K., Masanta M. Effect of overlapping condition on large area NiTi layer deposited on Ti-6Al-4V alloy by TIG cladding technique. *Surface and Coatings Technology*. 2020, 385: 125417.
 26. Lailatul P.H., Maleque M.A. Surface modification of duplex stainless steel with SiC preplacement using TIG torch cladding. *Procedia engineering*. 2017, 184: 737–42.
 27. Ghadami F., Sohi M.H., Ghadami S. Effect of TIG surface melting on structure and wear properties of air plasma-sprayed WC–Co coatings. *Surface and Coatings Technology*. 2015, 261: 108–13.
 28. Haldar B., Saha P. Identifying defects and problems in laser cladding and suggestions of some remedies for the same. *Materials Today: Proceedings*. 2018, 5(5): 13090–101.
 29. Van Acker K., Vanhoyweghen D., Persoons R., Vangrunderbeek J. Influence of tungsten carbide particle size and distribution on the wear resistance of laser clad WC/Ni coatings. *wear*. 2005, 258(1–4): 194–202.
 30. Singh J., Thakur L., Angra S. Abrasive wear behavior of WC-10Co-4Cr cladding deposited by TIG welding process. *International Journal of Refractory Metals and Hard Materials*. 2020, 88: 105198.
 31. Buytoz S., Ulutan M., Yildirim M.M. Dry sliding wear behavior of TIG welding clad WC composite coatings. *Applied Surface Science*. 2005, 252(5): 1313–23.
 32. Tosun G. Ni–WC coating on AISI 1010 steel using TIG: microstructure and microhardness. *Arabian Journal for Science and Engineering*. 2014, 39: 2097–106.
 33. Lin Y.C., Chang K.Y. Elucidating the microstructure and wear behavior of tungsten carbide multi-pass cladding on AISI 1050 steel. *Journal of Materials Processing Technology*. 2010, 210(2): 219–25.
 34. Dai Q.L., Luo C.B., You F.Y. Crack restraining methods and their effects on the microstructures and properties of laser clad WC/Fe coatings. *Materials*. 2018, 11(12): 2541.
 35. Ma Q., Li Y., Wang J., Liu K. Investigation on core-eutectic structure in Ni60/WC composite coatings fabricated by wide-band laser cladding. *Journal of Alloys and Compounds*. 2015, 645: 151–7.
 36. Yazdi R., Kashani-Bozorg S.F. Microstructure and wear of in-situ Ti/(TiN+ TiB) hybrid composite layers produced using liquid phase process. *Materials chemistry and physics*. 2015, 152: 147–57.
 37. Nowotny S., Berger L.M., Spatzier J. Coatings by laser cladding.
 38. Pawlowski L. Thick laser coatings: A review. *Journal of Thermal Spray Technology*. 1999, 8: 279–95.
 39. Liu Y.H., Li J., Xuan F.Z. Fabrication of TiC

- reinforced Ni based coating by laser cladding. *Surface Engineering*. 2012, 28(8), 560–3.
40. Cui C., Guo Z., Wang H., Hu J. In situ TiC particles reinforced grey cast iron composite fabricated by laser cladding of Ni–Ti–C system. *Journal of Materials Processing Technology*. 2007, 183(2–3): 380–5.
 41. Li Y., Bai P., Wang Y., Hu J., Guo Z. Effect of TiC content on Ni/TiC composites by direct laser fabrication. *Materials & Design*. 2009, 30(4), 1409–12.
 42. Shravan C., Radhika N., Deepak Kumar N.H., Sivasailam B. A review on welding techniques: properties, characterisations and engineering applications. *Advances in Materials and Processing Technologies*. 2023, 10: 80.
 43. Padilha A.F., Rios P.R. Decomposition of austenite in austenitic stainless steels. *ISIJ international*. 2002, 42(4): 325–7.
 44. Karaman I., Sehitoglu H., Maier H.J., Chumlyakov Y.I. Competing mechanisms and modeling of deformation in austenitic stainless steel single crystals with and without nitrogen. *Acta Materialia*. 2010, 49(19): 3919–33.
 45. Gavriljuk V.G. and Berns H. *High Nitrogen Steels*. Springer-Verlag, Berlin. 1999.
 46. Chumlyakov Y.I., Kireeva I.V., Korotaev A.D. Plastic deformation of single crystals of austenitic stainless steels strengthened by nitrogen. I: Orientation and temperature dependence of critical shear stress. *Physics of Metals and Metallography*. 1992, 73(4): 429–34.
 47. Chumlyakov Y.I., Kireeva I.V. and Ivanova O.V. *Phys. Met. Metall.* 1994, 78: 350.
 48. Hull D. and Bacon D.J. *Dislocations*. Oxford University Press, New York, 1989.
 49. Evangeline A, Sathiya P. Structure–property relationships of Inconel 625 cladding on AISI 316L substrate produced by hot wire (HW) TIG metal deposition technique. *Materials Research Express*. 2019, 6(10): 106539.
 50. Hassan K.A., Prangnell P.B., Norman A.F., Price D.A., Williams S.W. Effect of welding parameters on nugget zone microstructure and properties in high strength aluminium alloy friction stir welds. *Science and Technology of Welding and Joining*. 2003, 8(4): 257–68.